Bilayer and Trilayer Crystalline Formation by Collapsing Behenic Acid Monolayers at Gas/Aqueous Interfaces

Wei Bu* and David Vaknin*

Ames Laboratory and Department of Physics and Astronomy, Iowa State University, Ames, Iowa 50011

Received July 17, 2007. In Final Form: October 12, 2007

X-ray reflectivities and grazing incidence X-ray diffractions of behenic acid (BA) monolayers compressed to the collapse region reveal that the resulting structures are reproducible and exhibit a high degree of order. The structures of the collapsed monolayers depend on the subphase solution. On pure water, the collapsed monolayer forms a stable crystalline trilayer structure. For monolayers spread on Ca^{2+} solutions, we find that an inverted bilayer structure is formed; that is, stretched BA-Ca-BA (calcium dibehenate, with calcium ions bridging the polar headgroups) forms a monolayer with the hydrophobic tails in contact with the water surface.

I. Introduction

Recently, we reported on the structure of arachidic acid (AA) monolayers compressed to the collapse region by *in situ* surface sensitive neutron and synchrotron X-ray studies.[1] We found that the structures of the collapsed films depend on the subphase; that is, films that were manipulated on pure water or on Ca^{2+} solutions produced distinct structures upon collapsing. Insoluble monolayers at the gas/water interface (Langmuir monolayers) exhibit a variety of two-dimensional phases upon density manipulations (analogous to three-dimensional systems) such as gaslike phases and various liquid and solid phases.[2–6] The phases and structures of the relatively simple saturated fatty acids have been thoroughly explored and identified.[5–9] As the monolayer is compressed to a surface pressure (π) beyond a critical value, generally occurring at the minimal closely packed molecular area (i.e., the average cross section of the molecule A_0), the monolayer collapses and/or folds, forming a multilayered structure, and aggregates.[10–12] Our studies revealed that AA on pure water collapses by forming primarily a trilayer structure, with a high degree of in-plane crystallinity.[1] Although the trilayer structure on water has been suggested on different grounds, our structural studies have unambiguously confirmed it. When spread on divalent Ca^{2+} solutions, the collapsed AA film consists of an inverted bilayer and a trilayer mixture, whose final conformation depends on the compression protocol. The inverted bilayer, as we suggested,[1] consists of Ca-dimerized-arachidate, namely a monolayer formed by stretched AA-Ca-AA molecules such that the hydrocarbon tails are in direct contact with the water surface. Herein, we report on the collapse of behenic acid (BA) films to examine the general behavior of fatty acids upon collapse and the influence

of hydrocarbon chain length on the properties of the collapsed film. BA has two additional CH_2 units compared to AA, making the hydrocarbon tail ~2.5 Å longer than that of AA, rendering it a stronger hydrophobic character. Surface pressure versus molecular area (π–A) isotherms and synchrotron X-ray reflectivity and grazing incidence X-ray diffraction were conducted on films spread on pure water and on Ca^{2+} solutions before and after collapse.

II. Experimental Details

Monolayers of behenic acid ($CH_3(CH_2)_{20}COOH$, CAS No. 112-85-6, was purchased from Sigma Chemical Co.) were prepared at gas/aqueous interfaces in a thermostatic, solid Teflon Langmuir trough and spread from 3:1 chloroform/methanol solutions. $CaCl_2\cdot2H_2O$ was purchased from Sigma Inc. and used as provided. Ultrapure water (Millipore, Milli-Q, and NANOpure, Barnstead; resistivity, 18.1 MΩ cm) was used for all subphase preparations. Pure water and salt solutions were used without any buffer to adjust the pH (pH ~ 6.5). Compression of the monolayer was started 10–15 min after spreading the monolayer to allow for solvent evaporation. The monolayer was then compressed to a desired surface pressure at compression rates of 0.29–0.58 Å²/min, and the surface pressure was recorded by using a microbalance using a filter-paper Wilhelmy plate. To minimize radiation damage due to the formation of radicals and ions and to reduce background scattering from air, the films were kept in a water saturated helium environment during the synchrotron X-ray experiments. The trough is mounted on a motorized stage that can translate the surface laterally with respect to the incident beam, enabling illumination of different parts of the monolayer to monitor radiation damage, reproducibility, and sample homogeneity.

X-ray studies of the structures of films at gas/water interfaces were conducted on the Ames Laboratory Liquid Surface Diffractometer at the Advanced Photon Source (APS), beamline 6ID-B (described elsewhere[13]). The highly monochromatic beam (8.0 keV; λ = 1.5498 Å), selected by a downstream Si double crystal monochromator, is deflected onto the liquid surface to a desired angle of incidence with respect to the liquid surface by a second monochromator [α-Quartz ($10\bar{1}0$)] located on the diffractometer.[14]

X-ray reflectivity (XR) and grazing incidence X-ray diffraction (GIXD) techniques are commonly used to characterize the monolayer structure.[13,15–17] XR experiments yield the electron density (ED) profiles across the interface, and they can be related to molecular

* E-mail: vaknin@ameslab.gov (D.V.); weibu@iastate.edu (W.B.).

(1) Vaknin, D.; Bu, W.; Satija, S. K.; Travesset, A. *Langmuir* **2007**, *23*, 1888.
(2) Gaines, G. In *Insoluble Monolayers at the Liquid-Gas Interface*; Interscience: New York, 1966.
(3) Lundqvist, M. *Prog. Chem. Fats Other Lipids* **1978**, *16*, 101.
(4) MacRitchie, F. *Chemistry at Interfaces*; Academic Press Inc.: San Diego, CA, 1990.
(5) Kjaer, K.; Als-Nielsen, J.; Helm, C.; Tippman-Krayer, P.; Möhwald, H. *J. Phys. Chem.* **1989**, *93*, 3200.
(6) Bibo, A. M.; Knobler, C. M.; Peterson, I. R. *J. Phys. Chem.* **1991**, *95*, 5591.
(7) Kenn, R. M.; Boehm, C.; Bibo, A. M. *J. Phys. Chem.* **1991**, *95*, 2092.
(8) Durbin, M. K.; Richter, A. G.; Yu, C.-J.; Kmetko, J. M.; Bai, J. M.; Dutta, P. *Phys. Rev. E* **1998**, *58*, 7686.
(9) Kaganer, V.; Möhwald, H.; Dutta, P. *Rev. Mod. Phys.* **1999**, *71*, 779.
(10) Ries, H. E., Jr. *Nature* **1979**, *281*, 287.
(11) Smith, R. D.; Berg, J. C. *J. Colloid Interface Sci.* **1980**, *74*, 273.
(12) Mcfate, C.; Ward, D.; Olmsted, J. *Langmuir* **1993**, *9*, 1036.

(13) Vaknin, D. *Characterization of Materials*; Kaufmann, E. N., Ed.; Wiley: New York, 2003; Vol. 2, p 1027.
(14) Als-Nielsen, J.; Pershan, P. S. *Nucl. Instrum. Methods Phys. Res.* **1983**, *208*, 545.

arrangements in the film. The density profiles across the interface are extracted by refining a slab model that best fits the measured reflectivity by the nonlinear least-squares fit (NLSF) method. The ED profile $\rho(z)$ is constructed by a sum of error functions

$$\rho(z) = \frac{1}{2}\sum_{i=1}^{N+1} \mathrm{erf}\left(\frac{z - z_i}{\sqrt{2}\sigma_i}\right)(\rho_{i+1} - \rho_i) + \rho_1/2 \quad (1)$$

where $N + 1$ is the number of interfaces, $\rho_{i+1} - \rho_i$, z_i, and σ_i are the change in ED, the position, and the roughness of ith interface, respectively, ρ_1 is the ED of the subphase, and $\rho_{N+2} \approx 0$ is the electron density of the gas. The variable parameters are ρ_i, z_i (the thicknesses of slabs associated with different parts of the molecules are denoted as $d_i \equiv |z_i - z_{i-1}|$), and the roughness σ_i. The continuous ED is sliced into a histogram (several hundred slices) to compute the reflectivity by using the recursive dynamical method.[18,19]

GIXD measurements are conducted to determine the lateral organization in the film. In these experiments, the angle of the incident beam with respect to the surface, α, is fixed below the critical angle ($\alpha_c = \lambda(\rho_s r_0/\pi)^{1/2}$; $r_0 = 2.82 \times 10^{-13}$ cm, where ρ_s is the subphase ED) for total reflection, while the diffracted beam is detected at a finite azimuthal in-plane angle, 2θ, and out-of-plane angle, β (the angle of the reflected beam with respect to the surface). Rod scans along the surface normal at the 2D Bragg reflections enable the determination of the average ordered chain length and tilt angle with respect to the surface normal. The intensity along a rod scan of a 2D Bragg reflection is analyzed in the framework of the distorted wave Born approximation (DWBA)

$$I(Q_{xy}, Q_z) \propto |t(k_{z,i})|^2 |F(Q_z)|^2 |t(k_{k_f})|^2 \quad (2)$$

where $t(k_{z,i})$ and $t(k_{k_f})$ ($k_{z,i} = k_0 \sin\alpha$; $k_{z,f} = k_0 \sin\beta$) are the Fresnel transmission functions, which give rise to enhancements around the incoming (α) and outgoing (β) critical angles. The in-plane momentum transfer is given by $Q_{xy} = (Q_x^2 + Q_y^2)^{1/2}$.[20] In modeling, the length and the tilt angle are varied, and the intensities are adjusted for two tilt directions, toward nearest-neighbors (NN) and next NN (NNN).[5,15,21] The form factor for the tails is given by

$$F(Q_z') = \sin(Q_z'l/2)/(Q_z'l/2) \quad (3)$$

where Q_z' is defined along the long axis of the chain and l is the chain length. A position sensitive detector (PSD) in conjunction with a Soller slit system (divergence $\sim 0.1°$) was used for the GIXD studies.

III. Results and Discussions

A. $\pi-A$ Isotherms. Surface pressure versus molecular area ($\pi-A$) isotherms of behenic acid spread on pure water and on 10^{-1} M CaCl$_2$ solution demonstrate that the presence of Ca^{2+} affects the isotherm before and after collapse, as shown in Figure 1. Before collapse, at molecular areas slightly larger than the cross section of an acyl chain ($A_0 \approx 20$ Å^2), the isotherms indicate a distinct transition at surface pressure π_t from untilted to tilted acyl chains.[5] The addition of Ca^{2+} to the solution lowers π_t from
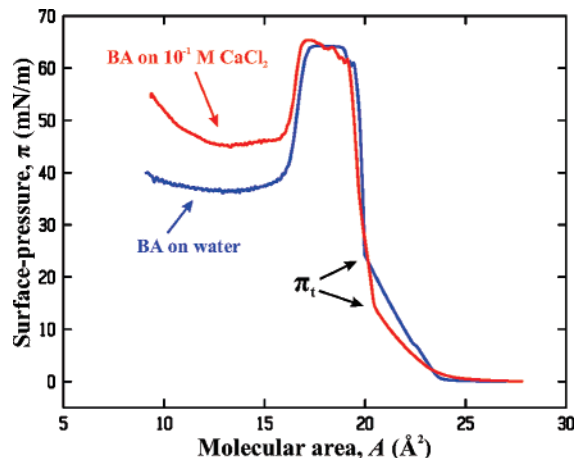
(15) Als-Nielsen, J.; Kjaer, K. In *Phase Transitions in Soft Condensed Matter*; Riste, T., Sherrington, D., Eds.; Plenum: New York, 1989.

(16) Vaknin, D.; Kjaer, K.; Als-Nielsen, J.; Lösche, M. *Biophys. J.* **1991**, *59*, 1325.

(17) Vaknin, D.; Kjaer, K.; Als-Nielsen, J.; Lösche, M. *Makromol. Chem.* **1991**, *46*, 383.

(18) Born, M.; Wolf, E. *Principles of Optics*; MacMillan: New York, 1959.

(19) Parratt, L. G. *Phys. Rev.* **1954**, *59*, 359.

(20) The coordinate system used in this manuscript is such that Q_z is normal to the liquid surface, Q_x is parallel to the horizontal (untilted) incident X-ray beam, and Q_y is orthogonal to both Q_x and Q_z. The hydrocarbon chains form two-dimensional polycrystals giving rise to a diffraction pattern that depends on the modulus of the in-plane momentum transfer $Q_{xy} = (Q_x^2 + Q_y^2)^{1/2}$ and is practically independent of sample rotation over the z-axis. We define $Q = (Q_{xy}^2 + Q_z^2)^{1/2}$ as the total momentum transfer.

(21) Kjaer, K. *Physica B* **1994**, *198*, 100.

Figure 1. Surface pressure versus molecular area of behenic acid on water and on 10^{-1} M CaCl$_2$ solution.

$\sim$24.2 to $\sim$14.1 mN/m for 10^{-1} M CaCl$_2$. The slopes of the isotherms, from the onset of finite surface pressures to π_t, are also found to be subphase-dependent. In the collapsed phase, both films initially give rise to a plateau in the isotherms, and as the films are compressed further the surface pressure falls off such that for the Ca^{2+} solution it is higher by $\sim$10 mN/m than that for BA on pure water. The overall features in the isotherms are similar to those observed in arachidic acid films;[1] however, the peak in the isotherm near the collapse point is much sharper for AA. The transitions observed in the isotherms, the peak, and the plateau after the peak for the collapse of fatty acids depend on subphase pH (i.e., interfacial pH) as already reported.[12] The addition of salts increases the interfacial pH due to the competition between the cations and protons,[22-24] and it seems to produce similar effects to pH manipulations.

B. X-ray Scattering from Behenic Acid on Pure Water. X-ray reflectivity measurements of BA on water and on solutions were conducted at various pressures before and after collapse. Figure 2A shows the reflectivity normalized to the reflectivity of an ideally flat water surface (R/R_F) of BA on water before collapse at $\pi \approx 30$ mN/m and after collapse. The solid lines in Figure 2A are calculated from the corresponding EDs shown in Figure 2B, the parameters of which are listed in Table 1. Before collapse, the total thickness of the monolayer is 29 Å, very close to the length of a stretched molecule. Indeed, the chain ($\sim$25.5 Å) is approximately 20 times the C–C bond length (1.27 Å) in acyl chains.[25] This strongly indicates that the chains, at this surface pressure ($\approx$30 mN/m), are normal to the water surface.

After collapse, BA forms an inhomogeneous film (the film was compressed to a nominal molecular area of $\sim A_0/2$, because of a limited compression ratio imposed by the Langmuir trough in our X-ray setup, and the inherent difficulty of producing a homogeneous trilayer). From the GIXD data, we determine that the film consists of a trilayer ($\alpha = 0.5$) and a monolayer ($1 - \alpha$), which agrees with the nominal molecular area of $\sim A_0/2$ obtained from the isotherm. Whereas X-ray reflectivity is well-defined for a homogeneous layered system, it is extremely complicated to evaluate for an inhomogeneous domainlike structure such as that in the present case of mono- and trilayer

(22) Israelachvili, J. *Intermolecular and Surface Forces*; Academic Press: London, 2000.

(23) Bu, W.; Vaknin, D.; Travesset, A. *Phys. Rev. E* **2005**, *72*, 060501(R).

(24) Bu, W.; Vaknin, D.; Travesset, A. *Langmuir* **2006**, *22*, 5673.

(25) Small, D. M. *The Physical Chemistry of Lipids: Handbook of Lipid Research*; Plenum Press: New York, 1986; Vol. 4.
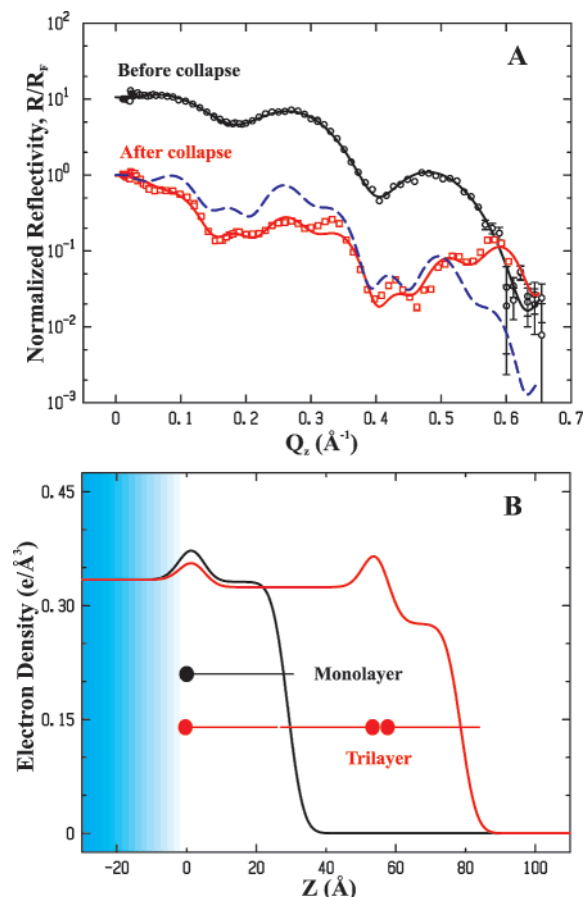
Figure 2. (A) Normalized X-ray reflectivities of behenic acid (BA) on pure water before (circles; shifted by a decade for clarity) and after collapse (squares). The solid lines are best-fit curves, as discussed in the text. The dashed line is calculated for the mixture with 50% monolayer and 50% trilayer. (B) Schematic structures (monolayer and trilayer) and electron densities used for fitting the corresponding reflectivity curves in (A).

Table 1. Parameters That Generate the Best-Fit Calculated Reflectivities to the Experimental Data for BA on Pure Water before and after Collapse[a]

	before	after[b]	
	monolayer	50% monolayer	50% trilayer
σ_0 (Å)	3.8 ± 2.0^c		
d_{head1} (Å)	3.5 ± 1.3	3.2 ± 1.3	3.5 ± 1.4
ρ_{head1} (e/Å^3)	0.437 ± 0.055	0.420 ± 0.040	0.398 ± 0.003
σ_1 (Å)	3.3 ± 0.3		
d_{chain2} (Å)	25.5 ± 1.7	25.3 ± 0.3	49.2 ± 2.2
ρ_{chain2} (e/Å^3)	0.331 ± 0.005	0.280 ± 0.005	0.324 ± 0.002
σ_2 (Å)	3.5 ± 0.1		
d_{head3} (Å)			4.0 ± 2.0
ρ_{head3} (e/Å^3)			0.444 ± 0.028
σ_3 (Å)			
d_{chain4} (Å)			22.0 ± 1.5
ρ_{chain4} (e/Å^3)			0.276 ± 0.002
σ_4 (Å)			

[a] Two- and four-slab models, for the monolayer and trilayer, respectively, are used to generate the ED profiles shown in Figure 2C. *[b]* For the film after collapse, we use same roughness instead of variable roughness for each interface, but this roughness is Q_z-dependent: $\sigma = 6.3-5.7Q_z$ Å. *[c]* In this work, the error estimation of a parameter is obtained by fixing a parameter at different values away from its optimum and readjusting all other parameters to a new minimum until χ^2 increased by 50%.

mixtures. We therefore caution that our analysis below cannot yield the exact ED of either constituent (mono- or trilayer). Our
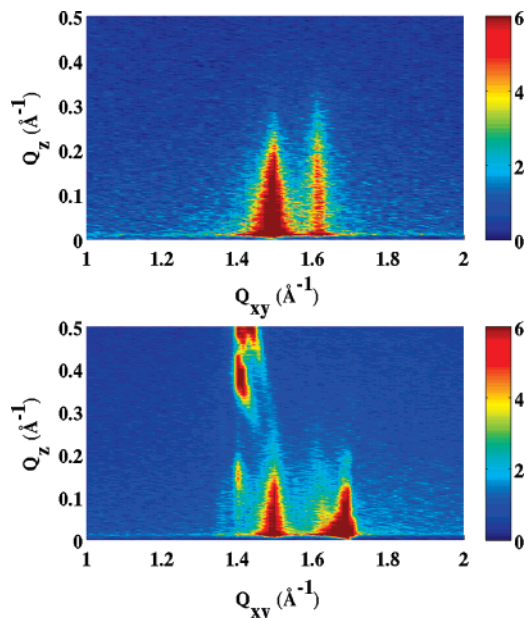

Figure 3. [Q_z:Q_{xy}] GIXD maps from BA on pure water before (upper panel) and after (lower panel) collapse. Q_z and Q_{xy} are out-of-plane and in-plane momentum transfers, respectively.

main goal is to show the existence of the trilayer, but not to extract its exact ED profile. The simplest approach is to assume that the reflectivity from a two-component system is the incoherent scattering sum

$$R_{mono}(Q_z) = \alpha R_{mono}(Q_z) + (1 - \alpha)R_{tri}(Q_z) \qquad (4)$$

where $R_{mono}(Q_z)$ and $R_{tri}(Q_z)$ are the reflectivities from the *presumably* homogeneous monolayer and trilayer, respectively. The dashed line in Figure 2A is calculated from the typical EDs of mono- and trilayers by using eq 4. Although the fit is not satisfactory, it surprisingly predicts the main observed features (e.g., the positions of the minima and maxima). It is interesting to note that the fit overestimates (underestimates) the reflectivity at low (high) Q_z values. This latter property prompted us to phenomenologically suggest that the average surface roughness (σ) which affects the reflectivity in a Debye−Waller form, namely, $R/R_F \sim e^{-Q_z^2\sigma^2}$, may be Q_z-dependent. Therefore, as a first approximation, we propose to expand σ to the linear term in Q_z

$$\sigma(Q_z) = \sigma_0 + c(Q_z) \qquad (5)$$

with the expectation that the refinement of an extra parameter will lead to $c < 0$. This modification, in fact, yields a much better agreement between the calculated and measured reflectivity, although at this time we do not understand the actual physical significance of this correction to the surface roughness. The solid line shown in Figure 2 is calculated using eq 5. The fit yields $\sigma_0 = 6.3 \pm 0.1$ Å, $c = -5.7 \pm 0.2$ Å^2, and a reasonable trilayer ED profile shown in Table 1. The total thickness of the trilayer film is $l_{tot} \approx 78.7$ Å, which is shorter than the stretched in-line three BA molecules ($l_{max} \approx 87$ Å). Assuming the trilayer film is tilted with respect to the surface normal collectively gives a tilt angle $t = \arccos(l_{tot}/l_{max}) \approx 25 \pm 7°$. A similar attempt to fit the reflectivity data of the collapsed film as the mixture of mono-, tri-, and five-layers just slightly improves the fit, but it shows that the presence of five-layer domains is less than 4%, suggesting that the five-layer domain is negligibly small. Moreover, rod scans in the GIXD pattern do not show any evidence of a five-layer phase.
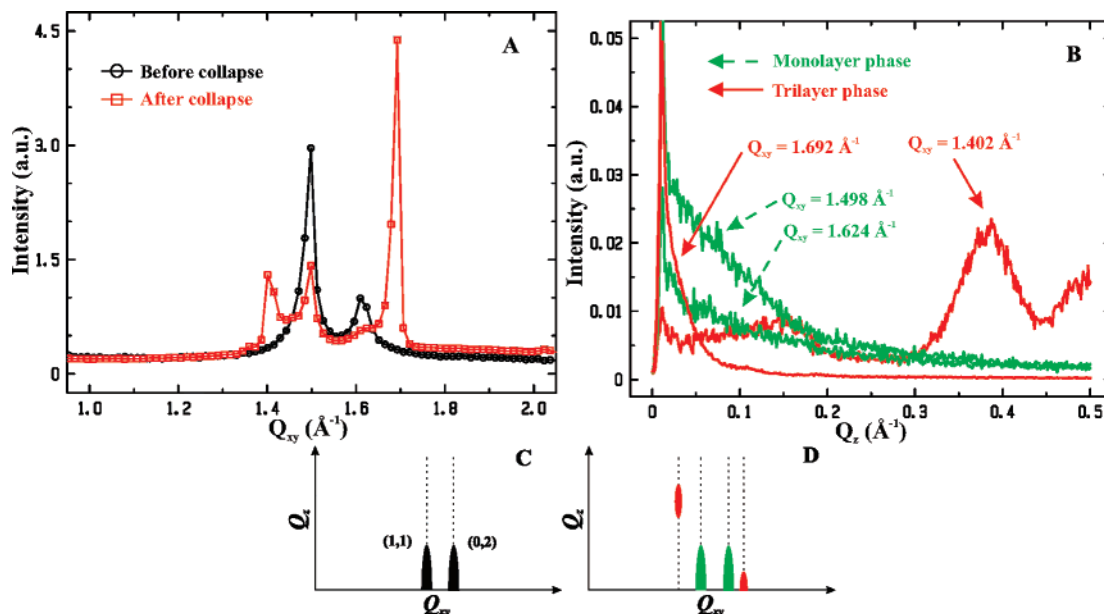
Figure 4. (A) Q_{xy}-cut of the GIXD map of BA on pure water before (circles) and after (squares) collapse. Solid lines are guides to the eye. (B) Four Q_z-cuts (rod scans) for BA on pure water after collapse at specific Q_{xy}'s as indicated, where peaks in (A) are observed. Schematic GIXD patterns for both before and after collapse are shown in (C) and (D), respectively.

Two-dimensional (Q_{xy}, Q_z) maps obtained from GIXD of BA on water before and after collapse ($Q_{xy} \equiv (Q_x^2 + Q_y^2)^{1/2}$) are shown in Figure 3. Before collapse (at 30 mN/m), we find that the diffraction pattern is relatively simple. It consists of two rodlike peaks, both associated with the in-plane ordering of the acyl chains. The two peaks have strong intensities near the $Q_z = 0$ plane, indicating the chains are not tilted, adopting the so-called herringbone structure.[9]

After collapse, the GIXD pattern looks more complicated, although it clearly shows the same two peaks of the monolayer structure phase, consistent with the inhomogeneous composition of the collapsed film ($\alpha = 0.5$). Several new peaks from the trilayer phase, both at $Q_z = 0$ and at $Q_z \neq 0$, indicate that the molecules, in the trilayer film, are ordered and tilted with respect to the surface normal, consistent with the analysis of the reflectivity above.

By examining Q_{xy}- and Q_z-cuts in the GIXD maps as shown in Figure 4A and B, we can obtain a more detailed picture of the structures (Figure 4C and D shows schematically the observations in Figure 3). Before collapse, the two in-plane peaks ($Q_{xy} = 1.494$ Å^{-1}, $Q_z = 0$; $Q_{xy} = 1.616$ Å^{-1}, $Q_z = 0$) are due to acyl chain ordering forming an in-plane centered rectangular unit cell. The two reflections can be indexed as a doubly degenerate (1,1) and a nondegenerate (0,2). The sublattice constants of the centered rectangular structure associated with the peaks are $a_s = 5.000$ Å and $b_s = 7.776$ Å, from which the chain cross section 19.44 Å^2 is derived (with two chains per unit cell). This can be compared with the isotherm (Figure 1) which yields ~19.7 Å^2 per molecule.

GIXD scans (squares, shown in Figure 4A) and rod scans (Figure 4B) after collapse indicate the presence of a monolayer phase, with two peaks as before collapse and another set of peaks due to the trilayer phase as discussed below. This indicates that the film is inhomogeneous, consisting of mono- and trilayer phases, as assumed in the analysis of the reflectivity. First, we contend that the two in-plane peaks after collapse ($Q_{xy} = 1.498$ Å^{-1}, $Q_z = 0$; $Q_{xy} = 1.624$ Å^{-1}, $Q_z = 0$) are associated with the monolayer phase. Figure 5 shows the rod scans after collapse ($Q_{xy} = 1.498$ Å^{-1}) and before collapse ($Q_{xy} = 1.494$ Å^{-1}) of

otherwise the same (1,1) reflection. Both scans are very similar except for a difference in intensity. The solid lines in Figure 5 are fits to the data using eq 2 with chain lengths $l \approx 25.2$ and 22.7 Å. Both values are consistent with the hydrocarbon chain thickness (~25.5 Å) for the monolayer structure as listed in Table 1. The inset in Figure 5 shows the intensity ratio between the rod scans before and after collapse up to the background level (up to $Q_z \sim 0.2$ Å^{-1}). The intensity ratio of the two rod scans is consistent with 50% monolayer coverage after collapse, as discussed in the analysis of the reflectivity above. This clearly shows that the rod scan at $Q_{xy} = 1.498$ Å^{-1}, after collapse, is from a monolayer phase.

The other peaks, in-plane ($Q_{xy} = 1.692$ Å^{-1}, $Q_z = 0$) and out-of-plane ($Q_{xy} = 1.402$, $Q_z = 0.384$ Å^{-1}), indicate the formation of a secondary trilayer phase. The in-plane sublattice unit cell, $a_s = 5.315$ and $b_s = 7.427$ Å, normal to the tilted chains yields a chain cross section of 19.74 Å^2. The average tilt angle of the chains from the surface normal can be calculated from the positions of the (1,1) and (0,2) peaks as follows:

$$\tan(t) = \frac{Q_z(1,1)}{\sqrt{Q_{xy}(1,1)^2 - (Q_{xy}(0,2)/2)^2}} \quad (6)$$

yielding $t \approx 19 \pm 1°$, where each chain is tilted toward its nearest-neighbor. This is consistent with the rough estimate obtained from the XR data ($\approx 25 \pm 7°$). Using eq 3, we estimate the film thickness l from the first minimum at $Q_z^{min} \sim 0.08$ Å^{-1} (of the rod scan at $Q_{xy} = 1.692$ Å^{-1}), where $l = 2\pi/Q_z^{min} \approx 78.5$ Å. This is about 3 times the monolayer thickness. Similarly, the film thickness can be estimated from the peak width of the rod scan at $Q_{xy} = 1.402$ Å^{-1} (the peak width is approximately 0.076 Å^{-1}), yielding ~82.5 Å. These, unequivocally, prove that the secondary phase after collapse is a trilayer.

C. Behenic Acid on CaCl$_2$ Solution. Figure 6 shows normalized reflectivities of BA on 10^{-1} M CaCl$_2$ solution before and after collapse. Before collapse, the reflectivity of the monolayer on Ca^{2+} solution is similar to that of BA on pure water, but overall it is more intense. Qualitatively, this is evidence
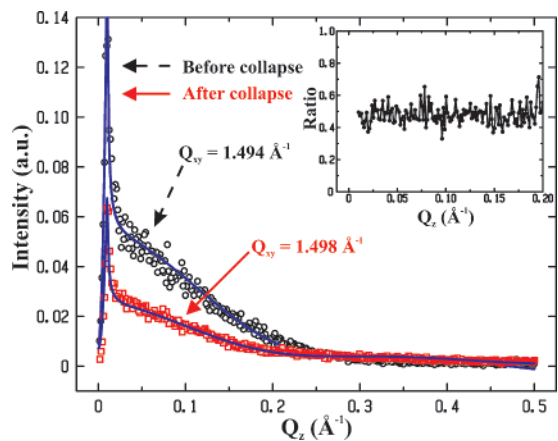
Figure 5. Rod scans before (circles) and after (squares) collapse at specific Q_{xy}'s as indicated. Solid lines are the best-fits obtained by using eq 2. Inset shows the intensity ratio between the two rod scans (after collapse and before collapse). The ratio indicates 50% monolayer coverage.
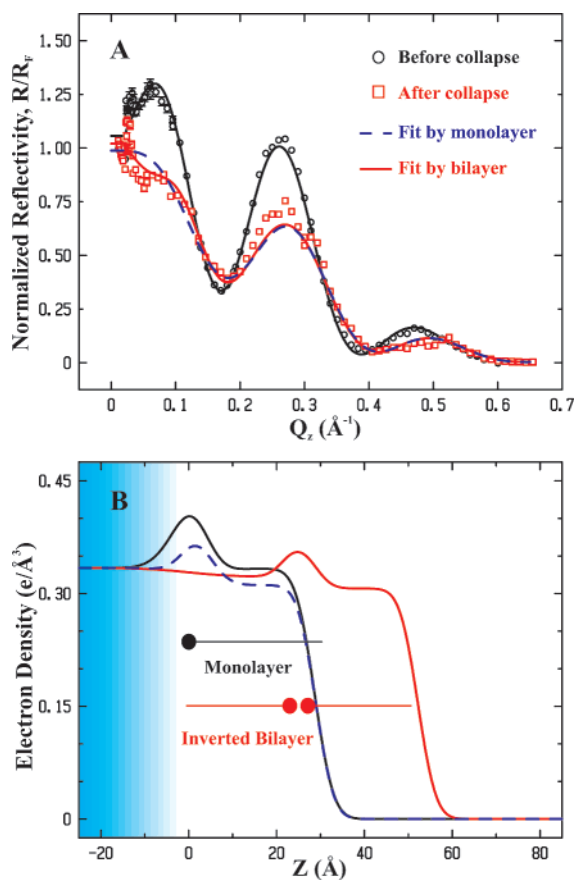

Figure 6. (A) Normalized X-ray reflectivities of behenic acid (BA) on 10^{-1} M CaCl$_2$ solution before (circles) and after (squares) collapse. The solid lines are best-fit curves as discussed in the text. The dashed line is the best attempted fit assuming a monolayer-like film with a two-slab ED model shown in (B). (B) Schematic structures (monolayer and inverted bilayer) and electron densities used for fitting the corresponding measured reflectivity curves in (A).

Figure 7. GIXD maps as in Figure 3 of BA on 10^{-1} M CaCl$_2$ before (upper panel) and after (lower panel) collapse.

Table 2. Parameters That Produce the Best-Fit Calculated Reflectivity to the Experimental Data for BA on 10^{-1} M CaCl$_2$ Solution before and after Collapse[a]

	before	after
σ_0 (Å)	5.2 ± 1.2	8.0 ± 5.8
d_{head1} (Å)	3.3 ± 0.6	
ρ_{head1} (e/Å^3)	0.556 ± 0.029	
σ_1 (Å)	3.7 ± 0.2	
d_{chain2} (Å)	25.4 ± 1.1	21.5 ± 2.0
ρ_{chain2} (e/Å^3)	0.333 ± 0.004	0.322 ± 0.002
σ_2 (Å)	3.4 ± 0.1	2.7 ± 1.1
d_{head3} (Å)		7.4 ± 2.0
ρ_{head3} (e/Å^3)		0.364 ± 0.012
σ_3 (Å)		2.9 ± 0.7
d_{chain4} (Å)		23.3 ± 1.7
ρ_{chain4} (e/Å^3)		0.307 ± 0.002
σ_4 (Å)		3.3 ± 0.1

[a] The two-slab model is used for the monolayer, whereas the three-slab model represents the bilayer after collapse. The same parameters are also used to show the EDs in Figure 6B.

significantly larger than that obtained for BA on pure water. A more detailed analysis, applying space-filling and volume constraints,[16,17,26,27] yields 0.45 ± 0.1 Ca^{2+} ions per BA molecule in the headgroup region. It is interesting to note that although the incorporation of Ca^{2+} to the headgroup region changes the ED of this region, it does not change its thickness significantly. This is consistent with similar observations for AA monolayers on Cd^{2+} solutions.[5]

The normalized reflectivity from the collapsed monolayer (squares shown in Figure 6) although surprisingly similar to the reflectivity before collapse has some subtle but reproducible differences. Compared to the reflectivity of the monolayer before collapse, the reflectivity after collapse has lower intensities overall and a minimum at $Q_z \sim 0.05$ Å^{-1}. The ED profile that produces the best-fit to the measured reflectivity is shown in Figure 6B, and the parameters are listed in Table 2. The relatively large error bar for σ_0 (Table 2) is due to the fact that the EDs on both

for an increase in the electron density in the monolayer (in the headgroup region) due to the incorporation of a bound Stern layer of Ca^{2+} ions at the carboxylic headgroup. The best-fit calculated reflectivity is obtained from the model ED shown in Figure 6B. The parameters used to fit the reflectivity data are listed in Table 2. The integrated ED of the headgroup region is
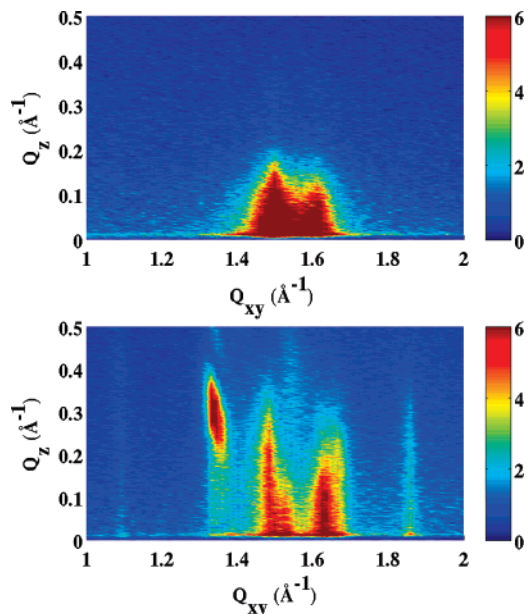
(26) Gregory, B. W.; Vaknin, D.; Gray, J. D.; Ocko, B. M.; Stroeve, P.; Cotton, T. M.; Struve, W. S. *J. Phys. Chem. B* **1997**, *101*, 2006.
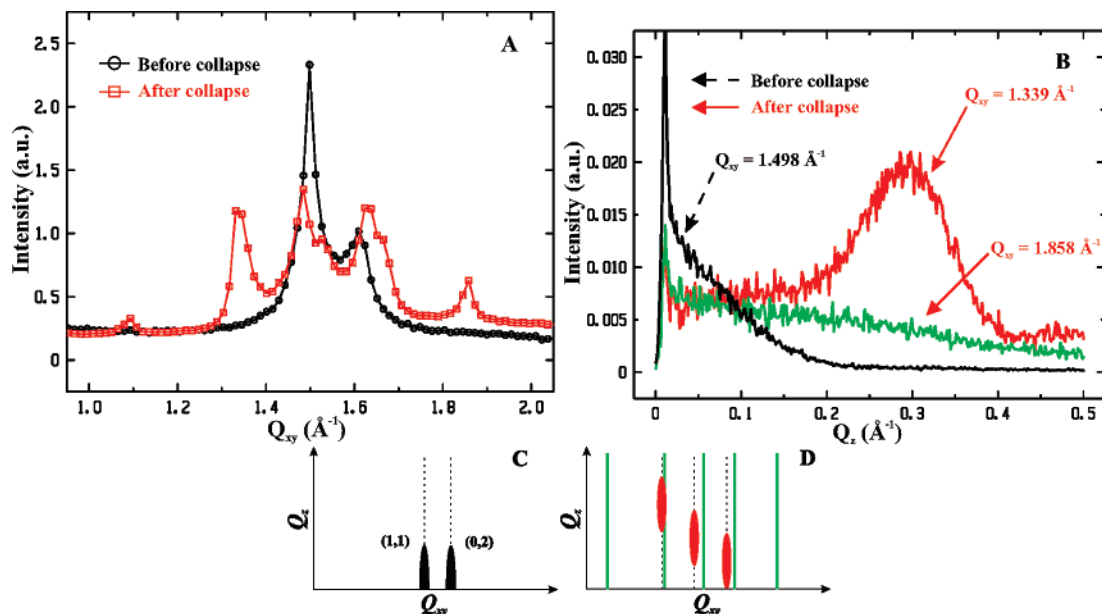(27) Vaknin, D.; Kelley, M. S. *Biophys. J.* **2000**, *79*, 2616.

Figure 8. (A) Q_{xy}-cut obtained from the GIXD map of BA on 10^{-1} M CaCl$_2$ solution before (circles) and after (squares) collapse. Solid lines are guides to the eye. (B) Three Q_z-cuts (rod scans) for BA on 10^{-1} M CaCl$_2$ solution before and after collapse at specific Q_{xy}'s as indicated, where peaks are observed in (A). Schematic GIXD patterns for both before and after collapse are shown in (C) and (D), respectively.

sides of this interface are very close (0.334 and 0.322 e/Å^3), and as is known from the Born approximation the reflectivity is most sensitive to changes in the ED, which for this interface is very small. We argue that the ED profile is consistent with the inverted bilayer structure, consisting of BA-Ca-BA with the hydrophobic tails of the stretched dimer in contact with the water surface (schematic configuration shown in Figure 6B). The film has a total thickness $d_{total} \sim 52.2$ Å, which is about twice that of the monolayer. The dashed line shown in Figure 6A is the best-fit assuming a monolayer-like structure. Although it is a reasonable fit, it can be ruled out, as it does not reproduce the minimum at $Q_z \sim 0.05$ Å^{-1} and the corresponding ED profile (dashed line in Figure 6B) is too low, in particular, in the headgroup region that includes the Ca^{2+} Stern layer. Other model structures, for example, trilayer and regular bilayer, did not produce good agreement between the calculations and the measured data or did not make physical sense.

Figure 7 shows GIXD patterns from BA monolayers on 10^{-1} M CaCl$_2$ solution before and after collapse. Before collapse, the pattern is quite similar to that of BA on pure water, except for slight differences in the intensities and peak positions along Q_{xy}. On the other hand, after collapse, the GIXD pattern is completely different from that for BA on pure water (lower panel in Figure 3), demonstrating that the addition of Ca^{2+} dramatically changes the in-plane structure in the collapsed region, most likely into a single phase, in accordance with the analysis of the reflectivity data. The GIXD pattern consists of long rodlike stripes and rods that peak at finite Q_z (i.e., more Q_z-dependent rods). We ascribe the stripes to the formation of quasi-2D crystals consisting of Ca and the carboxylic headgroups, and the Q_z-dependent rods with the in-plane long range ordering of the bilayer hydrocarbon chains.

A Q_{xy}-cut and several Q_z-cuts of the GIXD patterns and schematic GIXD patterns for both before and after collapse are shown in Figure 8A−D, respectively. Before collapse, the addition of Ca^{2+} does not affect significantly the chain ordering (there is no indication for long range order in the headgroup region of the film, consistent with numerous previous studies that show

the headgroup regions of monolayers are much less organized than the acyl chains). The two in-plane peaks at $Q_{xy} = 1.498$ Å^{-1}, $Q_z = 0$ and $Q_{xy} = 1.603$ Å^{-1}, $Q_z = 0$ indicate that the chains form a centered rectangular unit cell with sublattice constants of $a_s = 4.965$ Å and $b_s = 7.839$ Å, yielding a cross-sectional area 19.45 Å^2 per chain. The intensity along the $Q_{xy} = 1.498$ Å^{-1} rod is higher than that at $Q_{xy} = 1.603$ Å^{-1} due to simple multiplicities of the (1,1) and (2,0) peaks (four versus two, respectively).

Figure 8A shows the peaks for the collapsed film (squares), which can be distinguished by their corresponding rod scans into two sets of Bragg reflections: one (rodlike) associated with the headgroup ordering (calcium oxalate formation) and the other (peaked at finite Q_z) associated with the ordering of long acyl chains. Figure 8B shows two rod scans for the collapsed film: one at $Q_{xy} = 1.858$ Å^{-1}, associated with the headgroup ordering, decaying very slowly, and the other at $Q_{xy} = 1.339$ Å^{-1}, associated with the long acyl chain ordering, with a distinct maximum at finite Q_z. The thickness of the collapsed film can be estimated from the peak line width ($\Delta Q_z \approx 0.12$ Å), $d_{total} = 2\pi/\Delta Q_z \approx 52.4$ Å, in agreement with the $\sim$52.2 Å film thickness extracted from XR above. Analysis of other peaks in Figure 8A, also shown schematically in Figure 8D, leads to similar conclusions.

In the following, we demonstrate semiqualitatively the inference of layer thickness from the line shape of the rod scans. Equations 2 and 3 indicate that the intensity along the rod scan is proportional to $|F(Q_z')|^2$. Figure 9A shows calculations of the square of the form factor, eq 3, versus Q_z' for expected mono-, bi-, and trilayer thicknesses of $l = 26, 52$, and 78 Å, respectively. There are a couple of modifications to bear in mind before comparing these factors to observations, that is, Figure 9C. First, below $Q_z = 0$ ($Q_z < 0$), there is no intensity, as in the reflection mode the scattered beam is totally absorbed in the subphase. Second, the origin of the form factor may shift to $Q_z \neq 0$ if the chains are collectively tilted to a certain angle with respect to the surface normal. Using eq 6 and tilt angles of 16° and 19° for the bilayer and trilayer, respectively, we obtain the modified calculations shown in Figure 9B. Figure 9B demonstrates
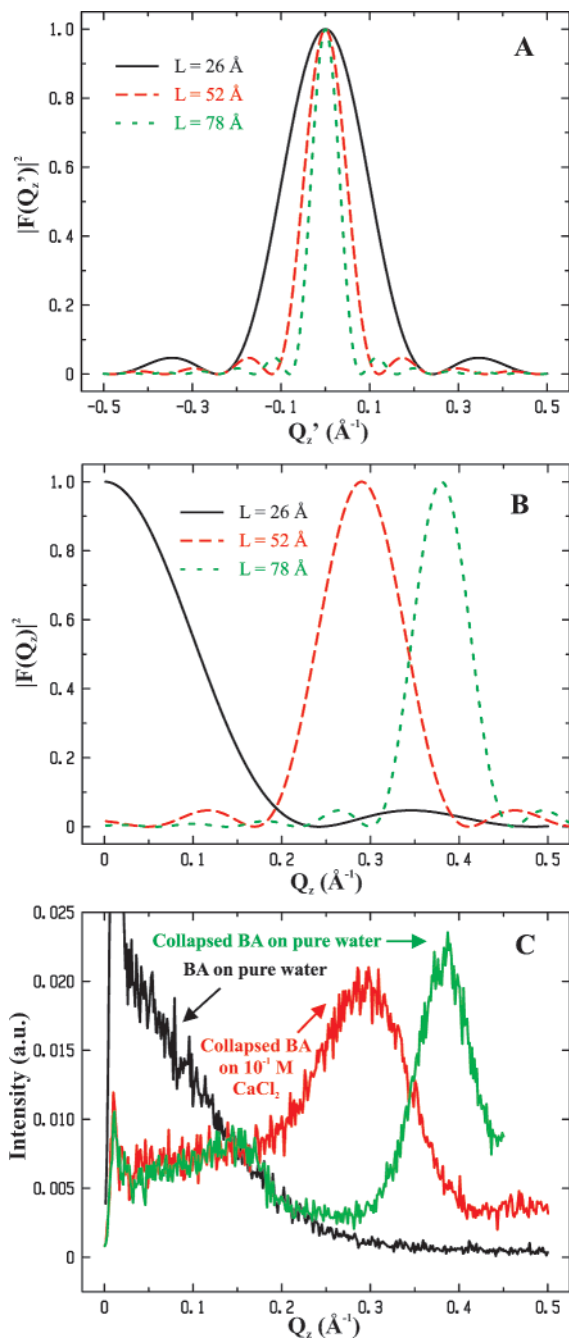
Figure 9. (A) $|F(Q_z')|^2$ versus Q_z' for three specific l values corresponding to expected mono-, bi-, and trilayer thicknesses as indicated. (B) Same as in (A), but the curves ($l = 52$ and 78 Å) are shifted along Q_z due to molecular tilts of 16° and 19°, respectively. (C) Rod scans for BA on pure water and Ca²⁺ solution both before and after collapse as indicated, showing the qualitative agreement with the calculated shapes shown in (B).

qualitative agreement with observations shown in Figure 9C, providing further evidence that the monolayer collapses by forming a trilayer and a bilayer structure for BA spread on pure water and on Ca²⁺ solution, respectively.

For comparison, Figure 10 shows normalized reflectivities from AA and BA spread on pure water (A) and on Ca²⁺ solution (B) in the collapsed region. Qualitative inspection shows that their overall shapes after collapse on the same subphase are very similar. However, they are very distinct when spread on pure water compared to Ca²⁺ solution. The main difference between BA and AA after collapse is that all minima and maxima of BA
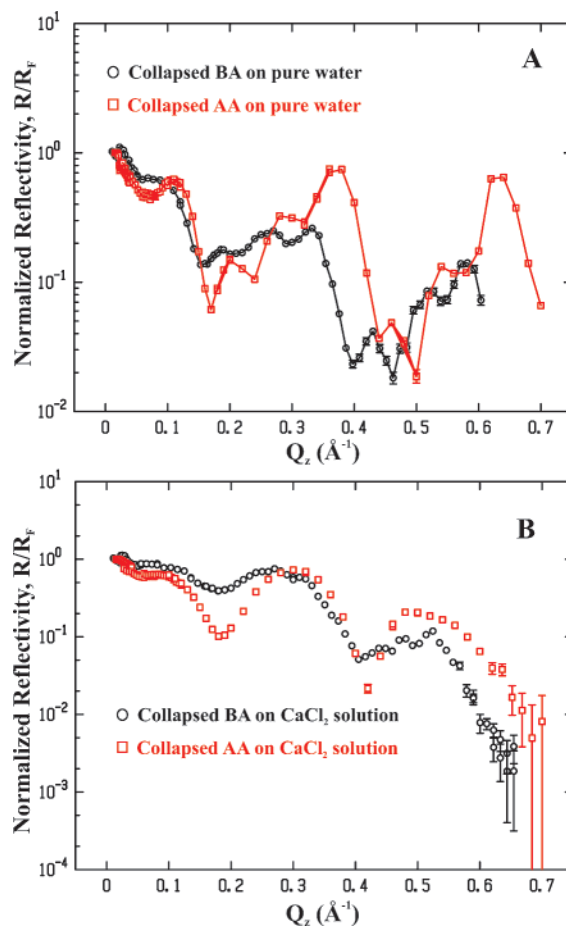

Figure 10. (A) Comparison of normalized reflectivities for AA and BA spread on pure water in the collapsed region (solid lines are eye guides). (B) Normalized reflectivities for AA and BA spread on Ca²⁺ solution in the collapsed region.

are shifted to smaller Q_z, which is simply due to the fact that BA has a longer chain.

IV. Conclusions

Using surface sensitive X-ray scattering studies, we determined the structures of BA films before and after collapse on pure water and on Ca²⁺ solutions. On pure water, BA collapses by forming primarily a trilayer structure. When spread and collapsed on Ca²⁺ solution, BA forms a relatively uniform inverted bilayer structure, that is, BA-Ca-BA with the hydrophobic tails in contact with the water surface. The GIXD data strongly suggest crystalline headgroup (calcium oxalate) formation. We point out that, unlike the case of AA, we did not observe a mixture state (bilayer and trilayer) as in our previous work.[1] The rationalization of the observed structures in terms of energetics is described elsewhere.[1,28]

(28) Lorenz, C. D.; Travesset, A. *Langmuir* **2006**, *22*, 10016.